Asian Journal of Chemistry; Vol. 34, No. 4 (2022), 841-848

ASIAN JOURNAL OF CHEMISTRY

https://doi.org/10.14233/ajchem.2022.23593

Electrochemical Activation of Nickel Oxide Incorporated Aluminum-Zinc Alloy Matrix as an Efficient Sacrificial Anode in Marine Environments

K.K. BINOJ

Department of Chemistry, Catholicate College (Affiliated to Mahatma Gandhi University, Kottayam), Pathanamthita-689645, India

Corresponding author: E-mail: kbinuk82@gmail.com, binoj_1982@yahoo.com

Received: 21 October 2021; *Accepted*: 12 December 2021; *Published online*: 10 March 2022; AJC-20724

For cathodic protection of steel, the aluminium-zinc alloy sacrificial anodes incorporated with nickel oxide nanoparticles were fabricated. The metallurgical properties of Al-Zn sacrificial anodes enhanced substantially through the infiltration and uniform dispersion of nickel oxide nanoparticles into an Al-Zn matrix. Such effective and uniform presence of nano nickel oxide inside the interior mass of the anodes was characterized by electrochemical techniques. The anodes showed considerably low polarization, steady and high active open circuit potential and substantially decreased self-corrosion during galvanic exposure for prolonged periods. The presence of nickel oxide nanoparticles in the anode matrix caused effective destruction of the passive aluminia film, which facilitated enrichment of galvanic performance of the anode. The anode had high resistance against biofouling also.

Keywords: Aluminium, Metal matrix composites, Corrosion, Polarization, Interfaces.

INTRODUCTION

The economic benefits of exploiting the low specific weight and high-current capacity of aluminium as an anode have been valued; however, on its surface, the spontaneous generation of a thin oxide film leads to a passivation effect. The thin oxide film formed in air becomes thicker with the production of hydrated species such as bayerite (Al $(OH)_3$) and bohemite (γ-AlOOH) when it is exposed to an electrolytic solution [1]. To promote activation, Al is alloyed with small amounts of elements, including Ga, In, Hg, Zn, Ce and Se, which shift the aluminium pitting potential to negative [2-6]. Most studies on this topic were performed on Al-rich Zn sacrificial anodes [7]. Zinc destabilizes oxide layers with $ZnAl_2O_4$ spinel formation [8]. The addition of 5% Zn to Al is reported to be optimum to synthesize sacrificial anodes because of high enhancement of the electrochemical and metallurgical characteristics of the alloy with β-phase formation [9]. Thus, the same alloy composition was used in this study.

Metal oxides play an important role in gas sensors, heterogeneous catalysis and corrosion. The addition of metal oxides in the Al alloy anode results in numerous improvements in its mechanical and physical properties. Metal oxide inclusion can improve grain boundaries, thereby alleviating grain boundary corrosion [10]. Aluminium and magnese oxides are used to fabricate high-wear-resistant sacrificial anodes [11]. Similarly, many metal oxides, including CeO_2, SiO_2, ZnO and ZrO_2, are also used to enhance both the galvanic and metallurgical characteristics of the Al-Zn alloy sacrificial anodes [12,13].

Nickel(II) oxide has been under extensive investigations as it has excellent catalytic and electrochemical properties [14-17]. The wide range of technological applications of nickel oxide includes sensors [18], lithium ion batteries cathodes [19], electrochemical super capacitors [20], electrochromic films [21] and catalysis [22]. Due to the quantum size, volume and surface effects, nanoscale nickel oxide exhibits many enhanced properties compared with microsized NiO. The structural properties (particle distribution, size, and morphology) of particles are closely associated with the used preparation techniques. Various methods, including sol-gel [23], micro emulsion [24], thermal decomposition [25], chemical precipitation [26] and amine-surfactant methods [27] are recommended for preparing NiO nanostructures. All these methods require high temperature, harsh growth conditions, and expensive experimental setup; are technically complex; frequently use organic components. Nanomaterial fabrication emphasises not only the size effect

but also the practicability and simplicity of synthesis techniques.

In this context, the present article highlights a simple and reliable process of electrochemical preparation of nano nickel oxide, its incorporation into Al-Zn alloy anode and their overall galvanic performance evaluation including electrochemical and morphological characteristics for the effective cathodic protection of steel substrates especially in marine environments.

EXPERIMENTAL

Fabrication of anode: Commercially available Zn (99.95%) and Al (99.75%) ingots were employed for casting the sacrificial anode of the Al + 5% Zn alloy. This combination of Zn and Al generates a homogeneous solid solution having grain boundaries and a uniform grain size throughout the crystal lattice. The alloy ingots were cut, weighed and melted in a graphite crucible, which was placed in a muffle furnace at 710 ±10 ºC. Various amounts of NiO (Sigma-Aldrich) nanoparticles were added to the melt and the mixture was stirred using a SiC rod for homogenization. At the same temperature, the melt was again placed in the muffle furnace for 15 min and then, it was poured into a pre-heated graphite die of 5.5 cm × 3.5 cm × 0.5 cm. The cast anodes were polished using various grades of the emery paper up to 600, were degreased using trichloroethylene, and washed with double-distilled water and dried.

Physico-chemical characterization: A Hitachi S- 2400 instrument was used to record scanning electron micrographs of the anode surface. For SEM analyses, the metallographic samples were cut from the centre of anode bulk. The samples were finely ground and then polished with 0.1 and 0.05 μm alumina slurry. In the polishing treatment, the metal was protected against galvanic deterioration by applying dehydrated ethanol for lubrication and then by ultrasonically cleaning with acetone. The samples were etched with 1% NaOH by immersing them into the NaOH solution for 30-60 s, washed using distilled water and dried. Finally, their secondary electron signal was examined. Anode hardness was estimated according to ASTM 384-89 by employing the Vickers micro-hardness indenter. With an indention time of 15 s, 980.7 mN test load was applied onto the anode surface. The hardness value was measured at different positions for each anode. The average values are presented in this work. The standard deviation was less than five Vickers harness units for all cases.

Electrochemical evaluation

OCP and CCP variation: The open circuit potential (OCP) of anode, *e.g*. the equilibrium potential established on the anode soon after its immersion in the respective electrolyte, was measured continuously with respect to saturated calomel electrode (SCE). The plot of time (60 days) *versus* OCP is presented as the change in the electrode-electrolyte interphase. At 30 ± 2 ºC, each anode was immersed in 3% NaCl solution. When the anode was coupled with a mild steel cathode and the couple was maintained dipped in 3% NaCl solution produced using analytical grade chemicals and distilled water, then with SCE, the closed-circuit potential (CCP) of the test anodes was constantly monitored for 60 days. An electrochemical cell was constructed to determine CCP; the anodes were placed in a specially designed cell, leaving an area of 10 cm^2 exposed. The dimensions of mild steel cathode was 11 cm × 4 cm × 0.5 cm and the distance between the electrodes were tunned as 3 cm. Parallel experiments were done in order to ensure reproducibility.

Potentiodynamic polarization: The cathodic and anodic polarization behaviour of the anodes was studied by linear sweep voltammetry using Autolab PGSTAT 30 corrosion measurement system. The analysis was carried out using 3% NaCl as electrolyte with electrodes of Ag/ AgCl, Pt and the Al-Zn alloy anode as reference, counter and working electrode, respectively. Potential sweep was done from ± 0.500 V from OCP. The system was allowed for one hour to stabilize the Al-Zn alloy anode in the electrolyte. Measurements were taken at scan rate of 0.010 V s^{-1}. The corrosion rate was determined by PGSTAT version 9.0 software.

Self corrosion: To measure the self-corrosion rate, the pre-weighed anode was immersed in 3% NaCl solution for 90 days at room temperature. The experiments were conducted according to ASTM G 31-72. The weight difference of the anodes after and before immersion was estimated after it was cleaned using the hot pickling solution of phosphoric acid (50 mL L^{-1}) and potassium dichromate (20 g L^{-1}). The anode was maintained mechanically and electrochemically undisturbed by using suitable insulation and supports. The corrosion rate was calculated on the basis of the weight loss data.

Galvanic efficiency: The accelerated electrochemical test was performed to determine the anode efficiency (ASTM G 97). The tests were conducted on the anode coupled with a mild steel cathode by impressing the anodic current density of 1 mA cm^{-2} (ratio of exposed area 1:10 cm^2) for 5 h in the aerated test solution containing simulated ocean water having the initial pH of 8.3, according to ASTM D 1141. The anode weight before and after immersion of respective galvanic coupling was measured after it was cleaned according to the ASTM G 31 standards. The theoretical current capacity of the anodes was calculated from the weight loss data. The actual current generated by the anode was estimated using the plot of current against time. The area under the graph was proportional to the real charge caused by the anode. The galvanic efficiency of the anode was determined using the formula:

$$\text{Efficiency } (\eta) = \frac{A}{B} \times 100$$

where A is the actual charge caused by the anode during the exposure period and B is the theoretical charge caused by the anode.

The test anode and a steel cathode with 10 times larger surface area were coupled with a copper wire. The top of the anode and surface electrical contact were insulated. Each similar couple with the anodes having a determined exposed surface area was immersed in 3% NaCl solution for 90 days. From actual current of the anode and the weight loss data, the galvanic efficiency was determined.

Electrochemical impedance characterization: Electrochemical impedance spectroscopy (EIS) provides considerable information about the corrosion reaction, mass transport, and

electrical charge transfer of anodes for conventional electrochemical polarization technique through interpretation and fitting of the impedance plot. EIS was performed with an electrochemical analyser (Auto lab PG stat 30 plus FRA 2). The Pt, Ag/AgCl (saturated) and the Al-Zn anode having 1 cm^2 exposed area were used as the counter, reference and working electrodes, respectively and 3% NaCl was used as the electrolyte. The impedance was analyzed with reference to OCP in the frequency of 1 MHz to 0.1 Hz after 60 min exposure of the anodes to the electrolyte.

Bio-growth characterization: Bio-growth on the anode was assessed by counting viable microorganisms on the anode surface caused by the exposure to natural seawater for 2 weeks exposure. The standard plate count method was used to determine total viable count (TVC). After 2 weeks, the biofilm produced on the anode surface was moved to peptone water. This mixture was shaken for 5 min to uniformly disperse the microorganisms in the medium. After 0.5 h, samples were diluted serially with sterile water to achieve 10^{-5} dilution. Onto the Zohell marine agar plates, 0.1 mL of sample from 10^{-5} dilution was spread. Table-1 presents the Zohell marine agar medium composition. The plates were incubated for 24 h at 37 ºC. The colony forming unit (CFU) was enumerated. The original count was calculated using the dilution factor as follows:

Microbial counts = Number of CFU × Dilution factor

RESULTS AND DISCUSSION

Microstructural analysis: The main objective of the present work was the metallurgical improvement as it is the main parameter, which can be significantly improved by means of nano nickel oxide incorporation. Fig. 1a-b evaluated the macrostructural optical microscopic characteristics of the Al-Zn anode and nano-nickel oxide incorporated Al-Zn anode while Fig. 1c-d shows that of SEM images, respectively. A significant difference in the morphology of two anodes was apparent during the analysis. The micrograph of the nano-nickel oxide incorporated Al-Zn anode also had uniform grain size with slight segregation of nickel oxide distributed regularly through out the entire surface. No other specific defects such as voids, cracks and channels were found. The smaller and uniform grain size could have large influence on the galvanic performance of the anode. Generally, anodes with small grains have high current capacity and efficiency [28]. Moreover, in present case, the whole area of Al-Zn anode was found relatively more defective than the nano-nickel oxide incorporated Al-Zn anode as there were many voids and cracks found on the former. Anodes having defective morphology usually lead to localized corrosion resulting low galvanic efficiency.

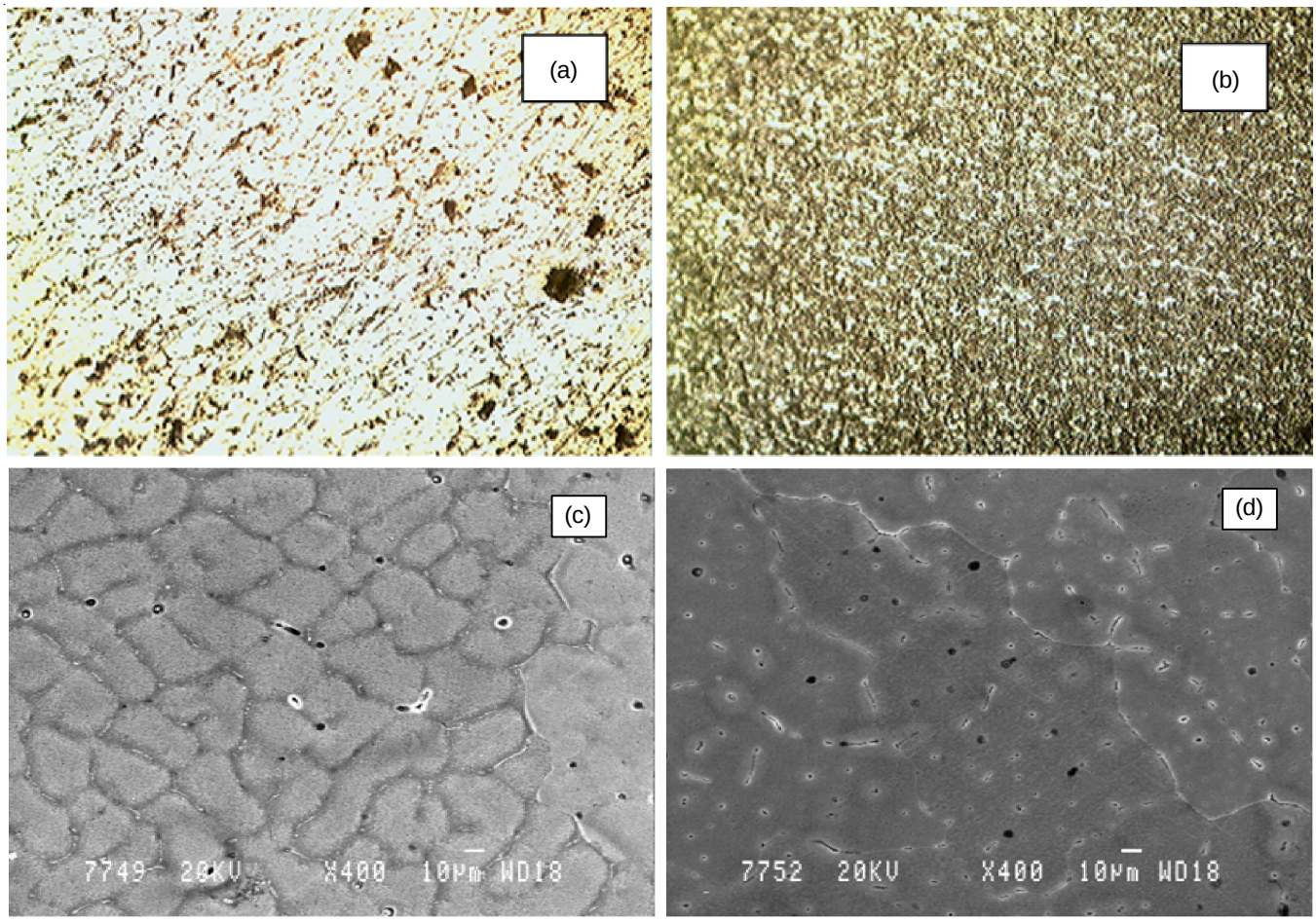

Fig. 1. Optical micrographs of the anode (a) Al-Zn, (b) nano NiO-incorporated Al-Zn, SEM micrographs of the anode (c) Al-Zn, (d) nano NiO-incorporated Al-Zn

TABLE-1
GALVANIC PERFORMANCE OF Al-Zn SACRIFICIAL ANODE INCORPORATED WITH DIFFERENT AMOUNTS OF NANO NICKEL OXIDE [Electrolyte: 3 % NaCl, Temp.: 30 ± 2 °C, stagnant condition]

Amount of nano nickel oxide (wt. %)	O.C.P. *vs.* SCE (V)	C.C.P. At i = 1 mA cm^{-2} (V)	Self-corrosion × 10^{-6} (g cm^{-2} h^{-1})	Efficiency (%)	Efficiency (i = 1 mA cm^{-2}) (%)
–	-0.950	-0.915	10.860	54	26
0.05	-0.950	-0.920	10.952	50	20
0.10	-0.955	-0.933	8.071	58	29
0.20	-0.960	-0.950	7.312	65	40
0.50	-0.982	-0.965	6.980	76	59
1.00	-0.967	-0.958	7.128	66	47

Hardness evaluation: The Vickers's hardness number of the 0.5% nano-nickel oxide incorporated Al-Zn anode was found to be 60 ± 2.7, which was slightly higher than that of pure Al-Zn anode (41 ± 1.4). The slight increase in the hardness was due to the dispersion of nano-nickel oxide particles to Al-Zn alloy matrix. The variation in the hardness numbers as a result of varying concentration of nano nickel oxide was found to be low in magnitude. The maximum concentration of nano nickel oxide was limited up to 0.5%, since higher amounts of nano-nickel oxide could decrease the energy density of the anode mass. It was also difficult to obtain a homogeneous alloy melt before casting, due to rejection of nano-nickel oxide in the melt. By means of nano-nickel oxide incorporation, the mechanical characteristics of the anodes were found slightly improved.

Electrochemical evaluation of anode

OCP characteristics: The open circuit potential (OCP) reliably represents the tendency of the anode to corrode. Fig. 2 presents the OCP decay trend of the anode incorporated with NiO nanoparticles (NPs) in 3% NaCl solution as the function of time. All the NiO NP incorporated anodes exhibited higher initial OCP than pure Al-Zn anodes (-0.950 V). Moreover, in all the NiO NP incorporated anodes, slight fluctuations in OCP values were observed only at the beginning of the test. Then, OCP values became nearly steady with the increase in the potential. This fluctuation in the potential was caused by the non-uniform corrosion of the anode, espec-ially in sacrificial anodes [21]. The OCP values of all the NiO NP incorporated anodes were between -0.953 and -0.982 V initially, and then, these values shifted between -0.912 and -0.951 V after two-month immersion. Compared with the pure Al-Zn anode, the anode with 0.5% NiO NPs showed the highest OCP with slight fluctuations in the potential (0.032 V) in the cathodic direction. The large shift in anodic OCP of the pure Al-Zn anode resulted from oxide film formation on the anode surface, which led to potential ennoblement [22]. Although all the anodes exhibited higher OCP than the pure Al-Zn anode, the optimum OCP one cannot be ensured on the basis of only these results. Thus, further analyses were conducted to study the galvanic performance of the anodes.

CCP variation: Closed circuit potential (CCP) is the potential of the anode when it is being consumed due to self anodic dissolution or oxidation during the cathodic protection of the coupled steel. Fig. 3 exhibited the trend of CCP variation of Al-Zn anodes incorporated with different amounts of nano

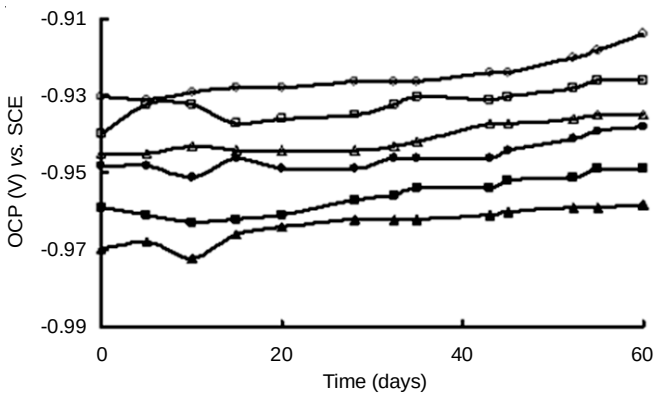

Fig. 2. OCP decay trend of Al-Zn alloy anode with different amounts of NiO NPs incorporation for a period of 60 days in 3 % NaCl solution (○) 0%, (△) 0.05%, (□) 0.1%, (●) 0.2%, (▲) 0.5%, (■) 1%

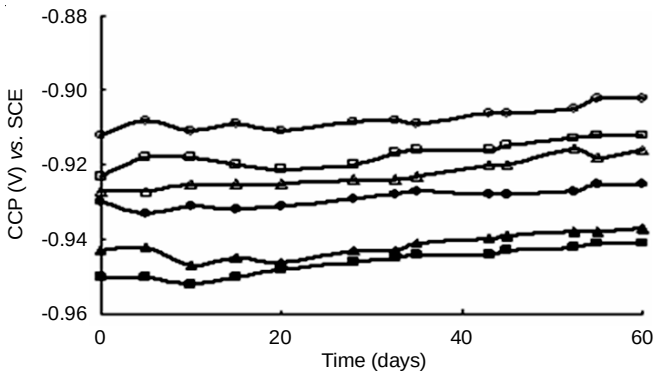

Fig. 3. CCP variation of Al-Zn anode with different amounts of NiO incorporation for a period of 60 days (cathode: mild steel, electrolyte: 3% NaCl) (○) 0%, (△) 0.05%, (□) 0.1%, (●) 0.2%, (▲) 0.5%, (■) 1%

nickel oxide under a current density of 1mA cm^{-2} for a time period of 60 days. All the nano-nickel oxide incorporated anodes showed high cathodic CCP values than the pure Al-Zn anodes, good agreement with initial CCP values displayed in Table-1. The anode incorporated with 0.5% nano-nickel oxide exhibited more active behaviour, in accordance with OCP values. Because a relatively noble potential indicates passivation, active CCP and OCP are desired for efficient sacrificial anodes. CCP values are measured only during the on-going galvanic reactions. Therefore, measuring the CCP variations during evaluation becomes important. The CCP values of all the anodes were in a narrow range, and hence, large inference was not obtained at this stage.

Potentiodynamic polarization: Typical potentiodynamic polarization curves of Al-Zn and nano-NiO incorportaed Al-

Zn alloy sacrificial anodes are shown in Fig. 4. The corrosion potential (E_{corr}) from -0.968 to -0.894 V *vs.* Ag/ AgCl. It was clearly seen that the incorporation of nano-nickel oxide into Al-Zn anode caused shifting of the corrosion potential to more negative values, which was desirable for effective cathodic protection systems. The polarization curve of pure Al-Zn anode was characterized by a broad passive region and also lower E_{corr} value due to the formation of protective oxide films on the aluminum surface. The current density varied from 3.141 to 3.106 A cm^{-2}. It was well known that the increase in I_{corr} represents the sacrificial action/ active nature of Al-Zn anode. The nano-NiO incorporated Al-Zn anode showed higher current density than pure Al-Zn anode confirms the significant enhancement of active nature of the Al-Zn sacrificial anode. The intermetallic phase if formed during the fabrication of the anodes was expected to act as additional cathodic sites that strongly foster the corrosive attack.

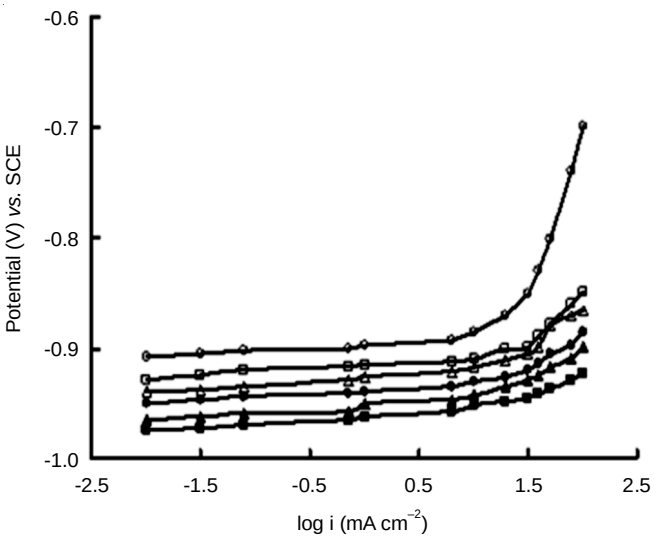

Fig. 4. Polarization behaviour of Al-Zn anode with different amounts of NiO incorporation in 3% NaCl solution (○) 0%, (△) 0.05%, (□) 0.1%, (●) 0.2%, (▲) 0.5%, (■) 1%

Inhibition of non-columbic metal loss: The major limitations of Al-Zn alloy sacrificial anodes include low galvanic efficiency and non-columbic metal loss. In this study, anodic self-corrosion was determined to determine the non-columbic metal loss, that is, the metal loss caused without it being utilised for sacrifice. Compared with the pure Al-Zn anode, all the NiO NP incorporated anodes showed low self-corrosion for 3 months in 3% NaCl solution (Table-1). For pure Al-Zn and NiO NP NP incorporated anodes, the self-corrosion values were 10.860 and 10.952-7.128 g cm^{-2} h^{-1}, respectively. Among all the NiO NP incorporated anodes, 0.5% NiO NP incorporated anode showed the minimum self-corrosion. To avoid frequent anode replacement, an efficient sacrificial anode should have low self-corrosion. The decreased self-corrosion values for the NiO NP incorporated Al-Zn anodes was attributed to the decrease in grain boundary corrosion because of enhanced grain refinement [8]. Moreover, the lack of other metallurgical imperfections including creaks and voids was the reason for high columbic efficiency and low self-corrosion.

Galvanic efficiency: Fig. 5 presents the comparison for the galvanic efficiency data of anodes with different amounts of NiO NPs. For the anode coupled with a mild steel cathode, the efficiency was estimated using the accelerated test with the impression of the anodic current density of 1 mA cm^{-2} for 5 h. The pure Al-Zn anode showed the efficiency of only 26%. The Al and Al alloys suffer from localized corrosion and pitting in a chloride environment. This is the chief reason for high self corrosion and low galvanic efficiency of Al anodes [7]. In this study, 0.5% NiO NP incorporated anode showed considerably high efficiency of 59%, indicating uniform anode dissolution. Theoretically, the uniform dissolution of anodes leads to the maximum efficiency. Secondary cathodic reactions on the interface surface or mechanical grain loss caused by local macro/ micro-corrosion cells caused the anode efficiency decline. The addition of high concentrations of NiO NP caused a drastic decline in the efficiency. Hence, the high concentration of NiO NPs was not incorporated.

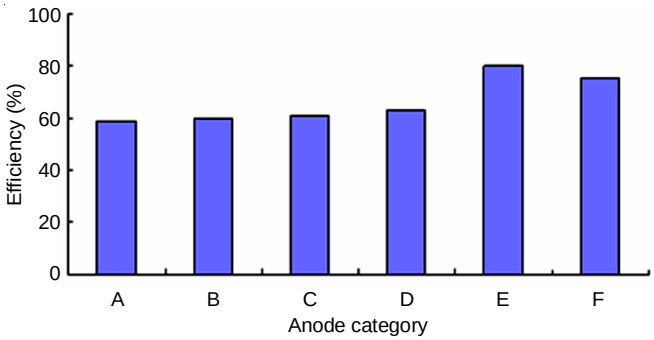

Fig. 5. Galvanic efficiency of Al-Zn anode with different amounts of NiO NPs incorporation (A) 0%, (B) 0.05%, (C) 0.1%, (D) 0.2%, (E) 0.5%, (F) 1%

The galvanic efficiency data of all the anodes for three months of immersion in 3% NaCl solution are shown in Table-1. All the anodes exhibited galvanic efficiency values in accordance with accelerated electro chemical test. Pure Al-Zn anode exhibited an efficiency of only 54%. On the other hand, 0.5% nano-nickel oxide incorporated anode had remarkably and relatively high efficiency as 76% during the accelerated tests. This revealed long-term uniform anode dissolution by the presence of nano-nickel oxide uniformly in the interior mass of anode during galvanic exposure. The galvanic efficiency of the anodes increased with increase in nano-nickel oxide concentration up to 0.5%. A gradual increase in the amount of nano nickel oxide prevented the formation of passive oxide film on the anode surface. Further, increase in the nano-nickel oxide content in the Al-Zn matrix reduced the galvanic efficiency due to the increase in the barrier properties of the anode surface. Thus it became clear that keeping the optimum concentration of nano nickel oxide (0.5%) was critical to get high efficiency of the anode.

Electrochemical impedance characterization: The EIS provided important information to explain the active behaviour of a complex corrosion system. The electrode impedance is a complex number. The impedance spectra are normally presented in the Nyquist (complex plane) plot, where the real part of

impedance (Z′) is plotted against imaginary part (-Z″). Fig. 6 shows the Nyquist plots of EIS data for nano-NiO incorporated and pure Al-Zn alloy sacrificial anode. From the impedance spectrum, it can be observed that Al-Zn a wide arc in the high frequency region. A similar trend was observed in the case of nano NiO NP incorporated Al-Zn anode also. However, the polarization resistance (R_p) values of nano NiO incorporated Al-Zn was found to be lower than that of pure Al-Zn anode. The polarization resistance (R_p) is an indication of effective interaction between the oxide film and the substrate, which lowers the surface resistance, a requisite to efficient sacrificial anodes [27]. The Nyquisite plot of pure Al-Zn reveals that the dominant and strong wide arc was due to thin alumina layer present in the outer most surface of metal alloy anode [29,30]. The impedance spectra also revealed that the incorporation of nano-NiO on Al-Zn anode led to destabilize the weak layer of aluminum oxide and the inner nickel oxide-aluminum layer, which was a favorable criterion for effective cathodic protection systems. It is well known that lower Z modulus at lower frequency displays better sacrificial action of the metal alloy anode [28]. As shown in Fig. 6, the Z modulus of nano NiO NP incorporated Al-Zn anode exhibited lower value and the linear slope modulus gradually decreased compared to that of pure Al-Zn anode.

Corrosion morphology: Corrosion of aluminum alloys usually occurs as a result of two major electrochemical reactions involving the anodic areas where metal dissolution occurs ($Al \rightarrow Al^{3+} + 3e^-$) and the cathodic areas where the reactions such as reduction of oxygen ($O_2 + 2H_2O + 4e^- \rightarrow 4OH^-$) occur. Fig. 7a-f illustrates the corroded surface of NiO NP incorporated Al-Zn anode for different immersion times. No large corrosion pits were observed (Fig. 7a). After 10 min immersion, a few pits with an average size of 4 µm appeared may be because of activation mechanism initiation (Fig. 7b). The solutions containing reactive ions, Al activation was initiated through pitting

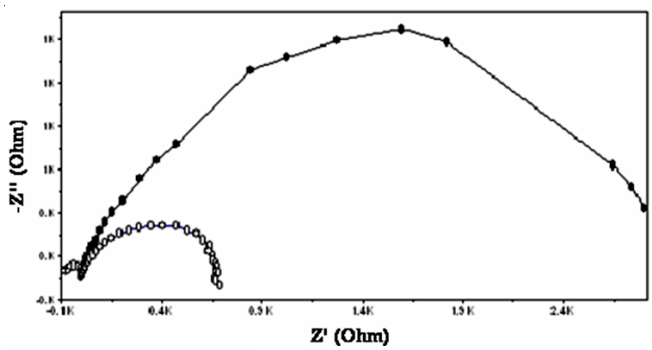

Fig. 6. Nyquist plots of (○) Al-Zn, (●) Al-Zn + NiO

at active sites. Subsequently, the flaw site of the anode surface, including precipitates, further caused the pitting propagation and initiation. Thus, the existence of small pits on the anode surface acted corrosion centre and was beneficial for the sacrificial activity of anode. For 1 h immersion, the pit size increased without any considerable increase in the pit number (Fig. 7c). In this scenario, no other precipitates appeared on the anode surface. After 10 h immersion, special features indicated mud-structured grains (Fig. 7d). On the anode surface, the mud structure could be explained by considering passivation as a dynamic process in the anode [6]. The oxide film was expected to dissolve and a fresh film was expected to generate at a slow rate. The freshly formed film on the pits was completely different from that observed in the growing pits of pure Al. This phenomenon depended on disso-lved cations, which may redeposit as hydroxides on the surface of the anode. After 3 days immersion, numerous pits and mud structures covered the anode surface (Fig. 7e). Till 30 days, these mud structures and pits spread around the almost entire anode surface (Fig. 7f). The metal-oxide based modification of Al alloys hampered the supply of oxygen and electron through barrier generation from the Al alloy surface to corrosion medium [21].

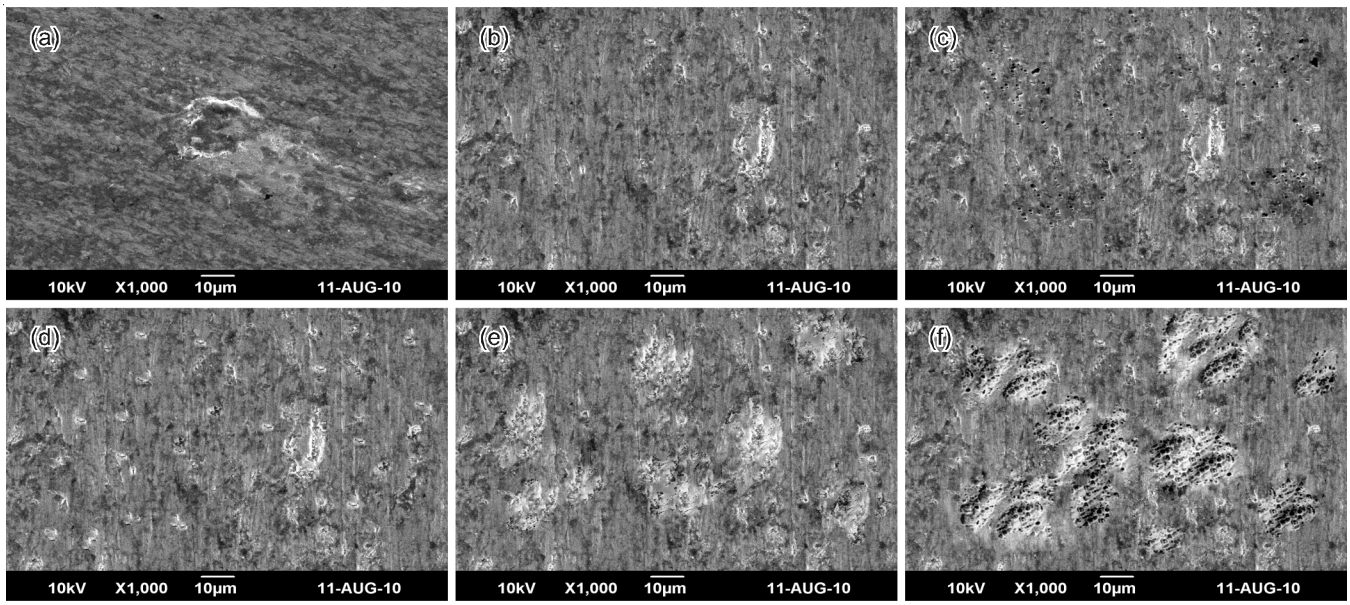

Fig. 7. SEM micrographs of Al-Zn anode incorporated with nano NiO after immersion in 3% NaCl solution for a period of (a) 10 min, (b) 30 min, (c) 1 h, (d) 10 h, (e) 3 days and (f) 30 days

In this case, a similar mechanism is assumed to occur between the corrosion medium and Al-NiO composite surface.

Effect of critical concentration of nano-NiO on the anode performance: The dependence of galvanic performance of Al-Zn alloy sacrificial anode and the critical concentration of nano nickel oxide was compared (Table-1). The incorporation of nano-nickel oxide into the Al-Zn matrix caused efficient activation and the effect of its critical concentration plays a crucial role in terms of metallurgical and galvanic characteristics of anode. The galvanic performance of anode substantially improves when the concentration of nano nickel oxide increases up to 0.5 wt.%, due to the effective degradation of surface lamina layer. Further increase in the concentration of nano-nickel oxide indicate an adverse effect, reduces the galvanic performance. The presence of higher concentrations of nano-nickel oxide led to the substantial reduction in self corrosion was inefficient to suppress the non-columbic metal loss during the galvanic process. Moreover, at high concentration of nano-nickel oxide may cause heterogeneity of the alloy melt prior to casting of the anode. The increased concentration of nano-nickel oxide in the matrix led to the over activation and localized corrosion,which is the main cause of low galvanic efficiency and high self-corrosion rate [6]. The barrier properties of anode surface also increase due to higher nano-nickel oxide deposition on the anode matrix. Thus, it became clear that keeping the optimum concentration of nano-nickel oxide on the anode matrix was critical to achieve high galvanic efficiency of anode.

Tolerance of anode in different aggressive media: The variation of the anode potential, OCP and CCP as a function of time when the anodes were immersed in aggressive chloride environments are shown in Fig. 8. As the concentration of NaCl solution increases from 3 to 10% both OCP and CCP values shifted to more negative region compared to pure Al-Zn anode.

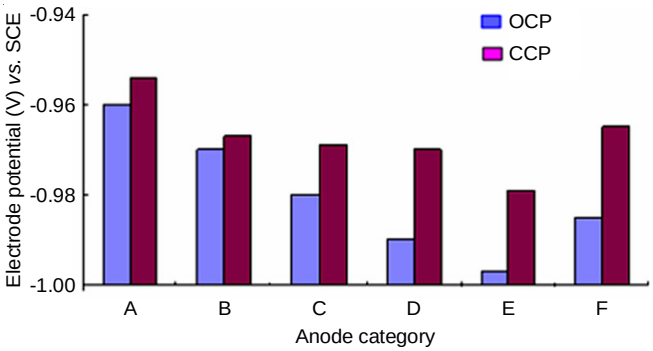

Fig. 8. OCP and CCP decay trend of Al-Zn alloy anode with different amounts of NiO incorporation in 10% NaCl solution (A) 0%, (B) 0.05%, (C) 0.1%, (D) 0.2%, (E) 0.5%, (F) 1%

In aggressive marine media, the cathodic reaction possible was hydrogen evolution either by dissociation of water molecules catalyzed by the Al_2O_3 film or chemical attack by OH^- and water accordingly as:

$$2H_2O \longrightarrow H_3O^+ + OH^- \quad (1)$$

$$2H_3O^+ + e^- \longrightarrow H_2 + 2H_2O \quad (2)$$

$$Al + OH^- + H_2O \longrightarrow AlO_2^- + 3/2H_2 \quad (3)$$

The released hydrogen react with anode surface to form substance such as AlH_3, AlH_2^+ and AlH^{2+}, which may shifts the potential to more negative region [5]. Moreover, oxide-film hydration occurs as a result of the local pH increase (alkalizing effect) at the interface oxide-solution with splitting of hydrogen from water. The hydrated region of the oxide film was considered to penetrate into the metal/oxide interface. This phenomenon led to the increase in the ionic conductance inside this part of the film and in the electron transfer rate (tunnelling) for the remaining anhydrous region. Finally, anomalous yield of hydrogen evolved at the bare metal because of the equivalent and simultaneous dissolution of the metal [9].

Bio-growth analysis: Biofouling has been recognized as a wide spread problem in design and operation of sacrificial anodes for marine applications. The tolerance of biofouling is a key factor that determines the worth of sacrificial anode in marine environments [7]. Biological organisms present in the marine environments often have the potential to increase or decrease oxygen support to the anode surface and consequently these organisms have critical role in affecting the performance of the anode. Adhesion of bacteria on solid surface is governed by electrostatic, van der Waals and Lewis acid base interactions. Both bacterial and solid surface properties like solid roughness, hydrophobicity, govern the initial adhesion phase of bacteria on the surface [5]. Fig. 9 shows the micrographs of the micro-organisms grown on Zohell marine agar developed from the bio-film. The number of cell colonies attached to pure Al-Zn anode was approximately 2600 CFU cm^{-2}, while the anode incorporated with the optimum amount (0.5%) of nano-NiO showed only 1400 CFU cm^{-2}. This remarkable reduction in cell colonies could be due to the reduction in solid roughness and change in solid surface chemical structure of the Al-Zn by nano-nickel oxide incorporation. Also with the increasing of nano-nickel oxide concentration, there was a significant reduction in bacterial reduction probably due to the formation of hydroxyl radical and hydrogen peroxide during enhanced oxygen reduction reactions. Thus, it was confirmed that nano-nickel oxide incorporation in Al-Zn matrix could effectively

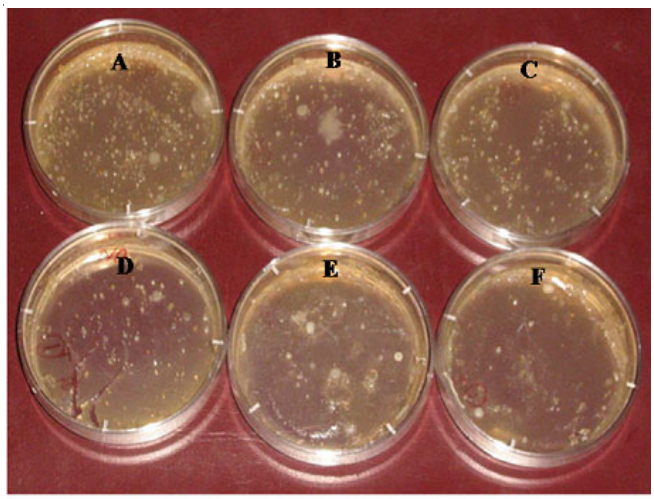

Fig. 9. Micrograph of biogrowth on Al-Zn anode with different amounts of NiO incorporation under natural marine conditions (A) 0%, (B) 0.05%, (C) 0.1%, (D) 0.2%, (E) 0.5%, (F) 1%

reduce biofouling and flourishing of microbial groups that interact in complex way to induce microbially induced corrosion.

Conclusion

An improvement in the metallurgical and galvanic characteristics of aluminum alloy anode could be achieved by the incorporation of nano-nickel oxide into the alloy. The optimum concentration of nano-nickel oxide is critical for the effective activation of the anodes. The metallurgical characteristics of the Al-Zn sacrificial anodes were improved substantially by means of uniform dispersion and infiltration of the nano nickel oxide particles into the Al-Zn matrix. Such an effective and uniform presence of nano nickel oxide inside the interior mass of the anode could be achieved by optimizing the experimental parameters. The anode incorporated with an optimum quantity (0.5%) of nano-nickel oxide exhibited high and steady negative OCP and CCP due to local thinning of passive oxide layer on the anode surface. It also caused very low polarization during galvanic exposure studies. High galvanic efficiency from 50 to 70% was achieved during accelerated tests due to the effective suppression of non-columbic metal loss and self corrosion due to nano-nickel oxide incorporation. The electro chemical impedance spectra revealed that the incorporation of nano-nickel oxide incorporation on Al-Zn sacrificial anode led to a substantial decrease in the polarization resistance (R_p) value, a favourable criterion for efficient sacrificial anodes. The present promising anodes have further merits in terms of easy development, economically viable, tolerance in aggressive media and bioresistance.

CONFLICT OF INTEREST

The authors declare that there is no conflict of interests regarding the publication of this article.

REFERENCES

1. A. Barbucci, P.L. Cabot, G. Bruzzone and G. Cerisola, *J. Alloys Compd.*, **268**, 295 (1998); https://doi.org/10.1016/S0925-8388(97)00605-1
2. D.O. Flamini, S.B. Saidman and J.B. Bessone, *Thin Solid Films*, **515**, 7880 (2007); https://doi.org/10.1016/j.tsf.2007.04.016
3. J.B. Bessone, D.O. Flamini and S.B. Saidman, *Corros. Sci.*, **47**, 95 (2005); https://doi.org/10.1016/j.corsci.2004.05.002
4. A.G. Munoz, S.B. Saidman and J.B. Bessone, *Corros. Sci.*, **44**, 2171 (2002); https://doi.org/10.1016/S0010-938X(02)00042-2
5. S.M.A. Shibli, B. Jabeera and R. Manu, *Mater. Lett.*, **61**, 3000 (2007); https://doi.org/10.1016/j.matlet.2006.10.062
6. S.M.A. Shibli, V.S. Dilimon and V.S. Saji, *J. Solid State Electrochem.*, **11**, 201 (2006); https://doi.org/10.1007/s10008-005-0088-5
7. S.M.A. Shibli and K.K. Binoj, *J. Appl. Electrochem.*, **39**, 159 (2009); https://doi.org/10.1007/s10800-008-9659-3
8. P.M. Ashraf and S.M.A. Shibli, *Electrochem. Commun.*, **9**, 443 (2007); https://doi.org/10.1016/j.elecom.2006.09.010.
9. B. Jabeera, T.S. Anirudhan and S.M.A. Shibli, *J. New Mater. Electrochem. Syst.*, **8**, 291 (2005).
10. Y. Wang, J. Zhu, X. Yang, L. Lu and X. Wang, *Thermochim. Acta*, **437**, 106 (2005); https://doi.org/10.1016/j.tca.2005.06.027
11. C. Shi, G. Wang, N. Zhao, X. Du and J. Li, *Chem. Phys. Lett.*, **454**, 75 (2008); https://doi.org/10.1016/j.cplett.2008.01.069
12. X. Xin, Z. Lü, B. Zhou, X. Huang, R. Zhu, X. Sha, Y. Zhang and W. Su, *J. Alloys Compd.*, **427**, 251 (2007); https://doi.org/10.1016/j.jallcom.2006.02.064
13. L. Xiang, X.Y. Deng and Y. Jin, *Scr. Mater.*, **47**, 219 (2002); https://doi.org/10.1016/S1359-6462(02)00108-2
14. S.M.A. Shibli, K.S. Beenakumari and N.D. Suma, *Biosens. Bioelectron.*, **22**, 633 (2006); https://doi.org/10.1016/j.bios.2006.01.020
15. P. Poizot, S. Laruelle, S. Grugeon, L. Dupont and J.-M. Tarascon, *Nature*, **407**, 496 (2000); https://doi.org/10.1038/35035045
16. X. Wang, J. Song, L. Gao, J. Jin, H. Zheng and Z. Zhang, *Nanotechnology*, **16**, 37 (2005); https://doi.org/10.1088/0957-4484/16/1/009
17. S. Illy-Cherrey, O. Tillement, J.M. Dubois, F. Massicot, Y. Fort, J. Ghanbaja and S. Bégin-Colin, *J. Mater. Sci. Eng. A*, **338**, 70 (2002); https://doi.org/10.1016/S0921-5093(02)00057-6
18. D.S. Wang, R. Xu, X. Wang and Y.D. Li, *Nanotechnology*, **17**, 979 (2006); https://doi.org/10.1088/0957-4484/17/4/023
19. M.T. Reetz, W. Helbig, S.A. Quaiser, U. Stimming, N. Breuer and R. Vogel, *Science*, **267**, 367 (1995); https://doi.org/10.1126/science.267.5196.367
20. X. Deng and Z. Chen, *Mater. Lett.*, **58**, 276 (2004) ; https://doi.org/10.1016/S0167-577X(03)00469-5
21. D.-L. Sun, B.-W. Zhao, J.-B. Liu, H. Wang and H. Yan, *Ionics*, **23**, 1509 (2017); https://doi.org/10.1007/s11581-017-1974-4
22. H. Sina, M. Emamy, M. Saremi, A. Keyvani, M. Mahta and J. Campbell, *J. Mater. Sci. Eng. A*, **431**, 263 (2006); https://doi.org/10.1016/j.msea.2006.06.011
23. S.Z. Abedin and F. Endres, *J. Appl. Electrochem.*, **34**, 1071 (2004); https://doi.org/10.1023/B:JACH.0000042672.23588.df
24. M.A. Talavera, S. Valdez, J.A. Juarez-Islas, B. Mena and J. Genesca, *J. Appl. Electrochem.*, **32**, 897 (2002); https://doi.org/10.1023/A:1020547508321
25. D.R. Salinas, S.G. Garcia and J.B. Bessone, *J. Appl. Electrochem.*, **29**, 1063 (1999); https://doi.org/10.1023/A:1003684219989
26. A. Venugopal and V.S. Raja, *Corros. Sci.*, **39**, 2053 (1997); https://doi.org/10.1016/S0010-938X(97)00082-6
27. S.M.A. Shibli and S. George, *Appl. Surf. Sci.*, **253**, 7510 (2007); https://doi.org/10.1016/j.apsusc.2007.03.052
28. J.H.W. de Wit and H.J.W. Lenderink, *Electrochim. Acta*, **41**, 1111 (1996); https://doi.org/10.1016/0013-4686(95)00462-9
29. L. Bai and B.E. Conway, *Electrochim. Acta*, **38**, 1803 (1993); https://doi.org/10.1016/0013-4686(93)80302-G
30. J.B. Bessone, D.R. Salinas, C.E. Mayer, M. Ebert and W.J. Lorenz, *Electrochim. Acta*, **37**, 2283 (1992); https://doi.org/10.1016/0013-4686(92)85124-4